Colloids and Surfaces B: Biointerfaces 129 (2015) 87–94

Contents lists available at ScienceDirect

Colloids and Surfaces B: Biointerfaces

journal homepage: www.elsevier.com/locate/colsurfb

Cubosome formulations stabilized by a dansyl-conjugated block copolymer for possible nanomedicine applications

Sergio Murgia[a,*], Angela Maria Falchi[b], Valeria Meli[a], Karin Schillén[c], Vito Lippolis[a], Maura Monduzzi[a], Antonella Rosa[b], Judith Schmidt[d], Yeshayahu Talmon[d], Ranieri Bizzarri[e], Claudia Caltagirone[a,*]

[a] Dipartimento di Scienze Chimiche e Geologiche, Università di Cagliari, S.S. 554 Bivio Sestu, I-09042 Monserrato (CA), Italy
[b] Dipartimento di Scienze Biomediche, Università di Cagliari, S.S. 554 Bivio Sestu, I-09042 Monserrato (CA) , Italy
[c] Division of Physical Chemistry, Department of Chemistry, Center for Chemistry and Chemical Engineering, Lund University, P.O. Box 124, SE-221 00 Lund, Sweden
[d] Department of Chemical Engineering, Technion–Israel Institute of Technology, Haifa 32000, Israel
[e] Istituto di Biofisica, CNR, U.O. Pisa, Via G Moruzzi 1, 56124 Pisa, Italy

ARTICLE INFO

Article history:
Received 19 September 2014
Received in revised form 23 January 2015
Accepted 9 March 2015
Available online 17 March 2015

Keywords:
Monoolein
Cubosomes
Theranostic nanomedicine
Pluronic F108
Fluorophores
Quercetin

ABSTRACT

We present here an innovative, fluorescent, monoolein-based cubosome dispersion. Rather than embedded within the monoolein palisade, the fluorescent imaging agent, namely dansyl, was conjugated to the terminal ethylene oxide moieties of the block copolymer Pluronic F108. We discuss the physicochemical and photophysical properties of this fluorescent Pluronic and of a cubosome formulation stabilized by a mixture of dansyl-conjugated and non-conjugated Pluronic, also including an anticancer drug (quercetin). Furthermore, we performed biocompatibility tests against HeLa cells to assess internalization and cytotoxicity features of this nanoparticles aqueous dispersion. Cryo-TEM, SAXS, and DLS analysis, proved the bicontinuous cubic inner nanostructure and the morphology of this fluorescent cubosome dispersion, while photophysical measurements and biocompatibility results basically validate their potential use for theranostic nanomedicine applications.

© 2015 Elsevier B.V. All rights reserved.

1. Introduction

Recent advances in nanomedicine resulted in the engineering of a number of nanoparticle systems based on hard and soft matter, able to simultaneously transport therapeutics and act as diagnostic agents. The new cross-discipline originating from these advances is known as theranostic nanomedicine [1–4]. With the purpose of enhancing the efficacy of the formulation, while reducing side effects, theranostic nanoparticles are designed for delivery to the site of disease, and within the same dosage, both pharmaceutically active molecules and imaging probes. This goal is often achieved by coating the surface of theranostic nanoparticles with a targeting ligand to specifically address the nanocarrier and its cargo to the pathological site. Additionally, this strategy of administration should allow to overcome the differences in biodistribution and selectivity of the two distinct entities represented by the drug and the diagnostic agent [5,6].

Monoolein (MO, glycerol monooleate) is a polar lipid that in water, besides a reverse micellar and a lamellar phase, originates two cubic bicontinuous liquid–crystalline phases, namely, the gyroid (C_G, space group *Ia3d*) and the double diamond (C_D, space group *Pn3m*), constituted by a curved, triply periodic, and non-intersecting MO bilayer, folded to form two disjointed continuous water channels [5–9]. The C_G and the C_D phases were virtually found ubiquitous in nature [10], and several papers were devoted to investigate the biological role of these nanostructures [10–13]. Remarkably, dispersion agents like Pluronics, nonionic poly(ethylene oxide)–poly(propylene oxide)–poly(ethylene oxide) (PEO–PPO–PEO) triblock copolymers, can be used to formulate these liquid–crystalline phases with cubic symmetry into stable colloidal dispersions in water, known as cubosomes [14,15]. It deserve noticing that colloidal dispersions characterized by a cubic inner structure are also formulated using other kinds of polar lipids (*e.g.*, phytantriol or mixtures of soy phosphatidylcholine and glycerol dioleate), and dispersants (*e.g.*, D-alpha-tocopheryl

* Corresponding authors. Tel.: +39 0706754453; fax: +39 0706754388.
E-mail addresses: murgias@unica.it (S. Murgia), amfalchi@unica.it (A.M. Falchi), meliv@unica.it (V. Meli), karin.schillen@fkem1.lu.se (K. Schillén), lippolis@unica.it (V. Lippolis), monduzzi@unica.it (M. Monduzzi), anrosa@unica.it (A. Rosa), sjudy@tx.technion.ac.il (J. Schmidt), ishi@tx.technion.ac.il (Y. Talmon), ranieri.bizzarri@nano.cnr.it (R. Bizzarri), ccaltagirone@unica.it (C. Caltagirone).

http://dx.doi.org/10.1016/j.colsurfb.2015.03.025
0927-7765/© 2015 Elsevier B.V. All rights reserved.

poly(ethylene glycol) 1000 succinate, or Polyoxyethylene (20) sorbitan monooleate) [16,17].

Cubosomes were only recently indicated as candidates for applications in theranostic nanomedicine [15,18,19]. Particularly, we demonstrated that cubosomes can be at the same time loaded with fluorophore probes (UV-visible or NIR emitting) and anticancer drugs (such as quercetin or camptothecin), and that they can be formulated with a mixture of Pluronic F108 (PF108) and folic acid-conjugated PF108 to make them cancer cell-specific targeted [20,21]. Among the numerous appealing features that can be exploited in theranostic nanomedicine, we can list the high structural stability and mechanical rigidity of cubosomes (due to their semi-rigid periodicity) they possess with respect to liposomes [22], their biodegradability (they are mainly prepared using monoolein, a biocompatible and biodegradable monoglyceride generally recognized as safe, GRAS, by the FDA) [23], and the possibility of carrying both hydrophobic and hydrophilic drugs. Importantly, their size fits perfectly that required in cancer therapy for the exploitation of the enhanced permeation retention (EPR) mechanism, while their PEG corona should prevent opsonization of these nanoparticles, thus slowing clearance from the bloodstream by the reticuloendothelial system [15,24]. Furthermore, in comparison with other lipid-based nanoparticles such as liposomes, cubosomes possess a huge interfacial surface area per unit of volume. Worth mentioning, *in vitro* investigations reported that components of the human plasma interact with the monoolein-based cubosomes provoking a cubic-to-hexagonal phase transition of the nanostructure [25,26]. According to SAXS experiments, such transition can be recorded few minutes after contact of the cubosomes with plasma, and it is completed after 1 h. Yet, an *in vivo* investigation of monoolein-based cubosomes loaded with a MRI contrast agent performed in rats, evidenced that the formulation, characterized by a half-life of about 90 min, was well tolerated, and successfully provided MRI contrast *in vivo* [18]. Therefore, independent of structure of the nanoparticles that finally reach the target tissue, the originally administered cubosome formulation was effective in delivering the imaging agent.

The formulation of functionalized cubosome dispersions is not trivial. Indeed, similarly to other self-assembled nanoparticles, cubosomes suffer of an intrinsic fragility. Therefore, even small amounts of additives used, for example, to impart them the desired features for nanomedicine application, may disturb the local surfactant dynamics, thus altering the original surfactant effective packing parameter with a consequent collapse of the cubic matrix [15,27]. In other words, additive loading may induce the transition toward other kinds of nanostructured dispersions, or to phase separation.

An innovative approach to confer cubosomes fluorescent properties while avoiding the impact of the imaging probe on the lipid bilayer was developed here. Particularly, the fluorophore, namely dansyl, was conjugated to the hydrophilic moieties of the PF108 used to stabilize the formulation. Given its solvatochromic properties, such a fluorophore was chosen to obtain further information on the nanostructure. In this paper, we discuss the physicochemical, photophysical, and HeLa cells internalization, and cytotoxic characteristics of this new cubosome formulation, also loaded with the anticancer drug quercetin.

2. Materials and methods

2.1. Chemicals

Monoolein (MO, 1-monooleoylglycerol, RYLO MG 19 PHARMA, glycerol monooleate; 98.1 wt %) was kindly provided by Danisco A/S, DK-7200, Grinsted, Denmark. The nonionic poly(ethylene oxide)–poly(propylene oxide)–poly(ethylene oxide) (PEO–PPO–PEO) triblock copolymer Pluronic PF108 with a block length composition of EO_{132}–PO_{50}–EO_{132} and an average molar mass of 14,600 g/mol, DMSO, Nile Red, MTT, quercetin, dansyl chloride (≥95%), potassium carbonate (99%), acetonitrile (≥99.9%), diethyl ether (≥99.5%), and dichloromethane (≥99%) were purchased from Sigma-Aldrich. Distilled water passed through a Milli-Q water purification system (Millipore) was used to prepare the samples.

2.2. Synthesis of dansyl-conjugated F108 (PF108-D)

K_2CO_3 (4 mg, 2.9×10^{-2} mmol) and dansyl chloride (6.3 mg, 2.32×10^{-2} mmol) were added to a solution of PF108–NH_2 (86 mg, 5.82×10^{-3} mmol) in anhydrous MeCN (5 ml), and the resulting mixture was refluxed under N_2 atmosphere overnight. The resulting turbid pale yellow solution was dried and the residue was dissolved in dichloromethane, filtered, and evaporated, under reduced pressure. The yellow oil obtained was washed with diethyl ether to eliminate excess dansyl chloride. The resulting yellow sticky oil was purified by dialysis (14 kDa MW cutoff) against deionized water, changed every 3–6 h for 3 days. The resulting product was lyophilized for 3 days to remove all of the residual water. Yield: 68% (60 mg, 3.94 mmol); mp: 49 °C. ^{1}H-NMR (400 MHz, DMSO-d_6, 298 K): δH 1.03 (d, J = 4 Hz; 3H × 50, —CH_3 of PPO), 2.83 (s, 3H × 4, -N(CH_3)$_2$ of the dansyl moieties) 3.48–3.55 (m, 3H × 50, 4H × 264, —CH_2—CH(CH_3)—O— of PPO and —CH_2—CH_2—O— of PEO), 4.50–4.65 (m, 1H × 2, sulphonamidic —NH), 7.10–7.30 (m, 1H × 2, amidic —NH), 7.7–8.2 (m, 6H × 2, aromatic protons).

2.3. Sample preparation

Monoolein-based cubosomes were prepared and stabilized by dispersing the appropriate amount of MO in water solutions of a 65/35 mixture of PF108/PF108-D using an ultrasonic processor UP100H by Dr. Hielscher (100 W, 30 kHz), at 90% of the maximum power with pulses of 1 s interrupted by 1 s breaks for 10 min. Doped cubosomes were obtained by dispersing the drug in the melted monoolein with the help of an ultrasonic bath before mixing with the Pluronic solution. The sample volume was usually 4 ml with approximately 96.4 wt% of water, 3.3 wt% of MO, and 0.3 wt% Pluronics mixture. Quercetin percentage was 3.3×10^{-4} wt%. SAXS experiments were performed on samples prepared with 92.8 wt% of water, 6.6 wt% of MO, and 0.6 wt% of Pluronic mixture.

2.4. Dialysis and drug loading efficiency

After loading with quercetin, the cubosome dispersion was purified from the non-encapsulated drug by dialysis: 2 ml were loaded into a dialysis tubing cellulose membrane (14 kDa MW cutoff) and dialyzed against water (1000 ml), for 2 h (by replacing the water after 1 h) at 5 °C. Drug loading efficiency (E%), expressed as percentage of the drug amount initially used, was determined by UV–vis spectroscopy after disruption of cubosomes with methanol. Quercetin content was quantified by a Thermo Nicolet Evolution 300 UV–vis spectrophotometer at 373 nm.

2.5. Cryogenic transmission electron microscopy

Cryogenic transmission electron microscopy (cryo-TEM) experiments were performed to visualize the cubosome nanoparticles. Vitrified specimens were prepared in a controlled environment vitrification system (CEVS) at 25 °C and 100% relative humidity. A drop (3 μl) of the sample was placed on a perforated carbon film-coated copper grid, blotted with filter paper, and plunged into

liquid ethane at its freezing point. More details about the methodology can be found elsewhere [28]. The vitrified specimens were transferred to a 626 Gatan cryo-holder and observed at 120 kV acceleration voltage in an FEI Tecnai T12 G^2 transmission electron microscope at about −175 °C in the low-dose imaging mode to minimize electron-beam radiation-damage. Typical electron exposures were 10 to 15 e-/Å^2. Images were digitally recorded with a Gatan US1000 high-resolution (2k × 2k pixels) CCD camera, using the DigitalMicrograph software.

2.6. Dynamic light scattering

For the determination of the size of the nanoparticles, the block copolymer micelles and unimers, as well as the ζ-potential of the nanoparticles, dynamic light scattering (DLS), and electrophoretic mobility measurements, respectively, were performed at either 25 °C or 50 °C (±0.1 °C) using ZetaSizer Nano ZSP (Malvern Instruments Ltd., Worcestershire, U.K.), which is equipped with a 10 mW helium–neon laser (operating at a wavelength of 633 nm). With this instrument, the DLS measurements are carried out at a fixed scattering angle $\theta = 173°$ using a backscattering technique. The electrophoretic mobility measurements are performed at $\theta = 17°$ using the M3-PALS (phase analysis light scattering) technique to detect the particle movement, which is used to calculate its electrophoretic mobility and from which the ζ-potential of the nanoparticles can be estimated [29,30]. The samples were put in disposable polystyrene cuvettes of 1 cm optical path length with Milli-Q water as solvent and the two types of measurements were thereafter conducted one after another, (DLS first). The cubosome nanoparticle samples were diluted 1:50 times prior to the measurements. The DLS measurements on the pure PF108 and PF108-D block copolymer solutions were performed without dilution at a concentration of 2.9×10^{-4}, and 3.8×10^{-4} M, respectively. The measured time correlation functions of the scattered intensity were analyzed using the software available in the Malvern instrument (CONTIN for PF108 and PF108-D block copolymer solutions) to obtain the intensity-weighted size distributions based on the apparent hydrodynamic diameter, d_H, which is calculated from the Stokes–Einstein relation $d_H = kT/6\pi\eta_0 D$, where D is the translational collective diffusion coefficient, obtained from the decay time of the correlation function, and η_0 is the viscosity of water. The reported d_H values correspond to an average of between three to five measurements. The DLS data were also analyzed using the cumulant method where the *Z*-average (intensity-weighted) d_H is calculated from the first cumulant from the second order analysis [31,32]. The polydispersity index (PDI) defined as the second cumulant, *i.e.*, the width of the size distribution, divided by the first cumulant squared was obtained in the cumulant analysis. For all systems and both techniques, at least two independently prepared samples were investigated.

2.7. Small-angle X-ray scattering (SAXS)

Small-angle X-ray scattering was recorded with a S3-MICRO SWAXS camera system (HECUS X-ray Systems, Graz, Austria). Cu Kα radiation of wavelength 1.542 Å was provided by a GeniX x-ray generator, operating at 50 kV and 1 mA. A 1D-PSD-50 M system (HECUS X-ray Systems, Graz, Austria) containing 1024 channels, 54.0 μm wide was used for detection of scattered X-rays in the small-angle region. The working *q* range (Å^{-1}) was $0.003 \leq q \leq 0.6$, where $q = 4\pi\sin(\theta)\lambda^{-1}$ is the scattering wave vector. For the analysis, thin-walled 2 mm glass capillaries were filled with the cubosome dispersions. The diffraction patterns of cubosomes were recorded for 3 h. The lattice parameter *a* of the cubic phases was determined using the relation $a = d(h^2 + k^2 + l^2)^{1/2}$ from linear fits of the plots of $1/d$ *versus* $(h^2 + k^2 + l^2)^{1/2}$, where $d = 2\pi/q$ (*q* is the measured peak position) and *h*, *k*, and *l*, are the Miller indices. Water channel radii were calculated using the relation $R_w = [(A_0/-2\pi\chi)^{1/2}a] - L$ [33], where *L* is the lipid length value (17 Å), *a* is the lattice parameter obtained from the SAXS analysis, and A_0 and χ are the surface area and the Euler characteristic of the infinite periodic minimal surface geometries (*Pn*3*m*, $A_0 = 1.919$, $\chi = -2$; *Im*3*m*, $A_0 = 2.345$, $\chi = -4$).

2.8. Photophysical characterization

Cubosome dispersions were diluted with Milli-Q water (1:6) and ultrafiltered with 450 μm filter before performing the photophysical measurements. The emission and excitation spectra were recorded with a PerkinElmer LS 55 spectrofluorimeter. The fluorescence quantum yield on PF108-D was determined by using the quinine sulphate dissolved in H_2SO_4 0.1 N as the reference standard ($\Phi_{ref} = 0.5654$). The absorption spectra were recorded on a Thermo Nicolet Evolution 300 spectrophotometer.

2.9. Cell culture

Human carcinoma HeLa cell line (ATCC collection) was grown in Phenol Red-free Dulbecco's modified Eagle's medium (DMEM, Invitrogen, USA) with high glucose, supplemented with 10% (v/v) fetal bovine serum, penicillin (100 U ml^{-1}), and streptomycin (100 μg ml^{-1}) (Invitrogen) in a 5% CO_2 incubator at 37 °C. Cells were seeded in 35 mm dishes, and experiments were carried out 2 days after seeding, when cells had reached 90% confluency. Cubosomes (1:500, 2 μl of formulation in 1 ml of medium) were added to the cells and incubated at 37 °C for 4 h. Live cell imaging experiments were performed as follows. The cubosome suspension was initially replaced with fresh serum-free medium, and then cells were loaded with the fluorescent probe Nile Red (NR). The fluorescent probe was washed out before the imaging session.

2.10. Fluorescence microscopy

Cells were stained with 300 nM NR (9-diethylamino-5H-benzo[a]phenoxazine-5-one) for 30 min. Microscopy observations were made with a Zeiss (Axioskop) upright fluorescence microscope (Zeiss, Oberkochen, Germany) equipped with 10×, 20×, and 40×/0.75 NA water-immersion objectives and an HBO 50 W L-2 mercury lamp (Osram, Berlin, Germany). Twelve-bit-deep images were acquired with a monochrome-cooled CCD camera (QICAM, Qimaging, Canada) with variable exposure. For the observation of the NR probe, the filters were ex 470 ± 20 nm and em 535 ± 40 nm for nonpolar lipids, and ex 546 ± 6 nm and em 620 ± 60 nm, for total lipids. Image alignments were obtained with Image Pro Plus software (Media Cybernetics, Silver Springs, MD).

2.11. Lipid droplet quantification

Cells, after nanoparticle treatments, were stained with NR. The latter is an ideal probe for the detection of lipids, as it exhibits high affinity, specificity, and sensitivity, to the degree of hydrophobicity of lipids. The latter feature results in a shift of the emission spectrum from red to green in the presence of polar, and nonpolar lipids, respectively. For this reason, in staining live cells with NR, cytoplasmic membranes are stained red, whereas neutral lipids of lipid droplets are stained green. Measurements, made on a single-cell basis, concerned the amount of lipid droplet content, evaluated by the fluorescence intensity of NR-green emission. The IOD (integrated optical density) per cell was calculated using the Image ProPlus software.

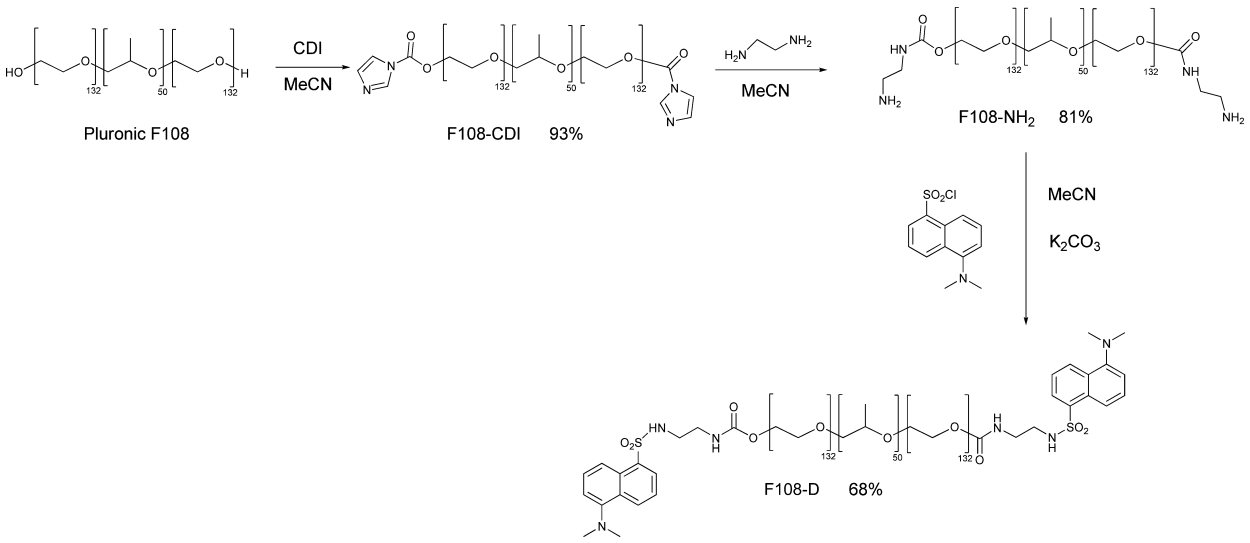

Scheme 1. Reaction scheme for the synthesis of F108-D.

2.12. Cytotoxic activity: MTT assay

The cytotoxic effect of nanoparticle formulations was evaluated in HeLa cells by the MTT assay. HeLa cells were seeded in 24-well plates at density of 3×10^4 cells/well in 500 μl of serum-containing media. Experiments were carried out 2 days after seeding when cells had reached 90% confluence. Cubosomes were added to the cells at a concentration of 1:500 (2 μl of sample in 1 ml of serum-free medium) and incubated at 37 °C for 4 h. A 50 μl portion of MTT solution (3-(4,5-dimethylthiazol-2-yl)-2,5-diphenyltetrazolium bromide) (5 mg/ml in H_2O), was then added and left for 2 h at 37 °C. The medium was aspirated, 500 μl of DMSO was added to the wells, and color development was measured at 570 nm with an Infinite 200 auto microplate reader (Infinite 200, Tecan, Austria). The absorbance is proportional to the number of viable cells. All measurements were performed in quadruplicate and repeated at least three times. Results are shown as percent of cell viability in comparison with non-treated control cells.

2.13. Statistics

Statistical analysis was carried out with Excel (Microsoft Co., Redmond, WA) or Graph Pad INSTAT software (GraphPad software, San Diego, CA). Results were expressed as a mean ± standard deviation (SD) of two independent experiments involving duplicate analyses for each sample. Statistically significant difference was evaluated by two sample *t*-tests with $p < 0.05$ as a minimal level of significance, or using one-way analysis of variation (One-way ANOVA) and the Bonferroni Post Test.

3. Results

3.1. Fluorescent cubosome formulation and physicochemical characterization

The block copolymer Pluronic F108 (PF108) was synthetically modified as recently reported in the literature [20], by reaction with ethylenediamine after activation with CDI (carbonyldiimidazole) to obtain PF108-NH_2. The aminated derivative was then reacted with commercially available dansyl chloride in anhydrous MeCN in the presence of K_2CO_3 as a base (Scheme 1). The sulfonamide derivative PF108-D was obtained in 68% yield. To avoid significant alterations of the pristine cubosome characteristics, the fluorescent block copolymer PF108-D was used to stabilize the formulation in mixture with the non-conjugated PF108. Preliminary tests indicated this mixture to be adequate in the ratio PF108/PF108-D = 65/35. The cryo-TEM images of the monoolein colloidal dispersion stabilized with such a mixture (cubosomes-D), encapsulating an anticancer drug, namely quercetin, are shown in Fig. 1. Quercetin loading efficiency (*E*%) was found to be 80%.

The cryo-TEM direct images of the nanoparticle dispersions reveal a colloidal dispersion consisting of nanoparticles of a diameter varying in the range from about 50 to 300 nm, characterized by a highly ordered inner nanostructure consistent with that expected for cubosomes. From a morphological point of view, along with many cubic-shaped nanoparticles, numerous round-shaped cubosomes were also observed. Moreover, as previously reported in the literature, cryo-TEM images also show several small unilamellar vesicles as well as nanoparticles where the so-called inter-lamellar attachments can be clearly seen. [34]

SAXS was used to confirm the cubic symmetry of the nanoparticles. To improve the signal-to-noise ratio, these experiments were performed on samples formulated with 7.2 wt% of the dispersed phase (MO + PF108/PF108-D mixture, see also paragraph 2.3). The diffraction patterns reported in Fig. 2 revealed the coexistence of two phases identified through at least two Bragg peaks with relative positions in a ratio of $\sqrt{2}:\sqrt{3}$, which we indexed as the (110) and (111) reflections of a double diamond inverse bicontinuous cubic phase ($Pn3\,m$ crystallographic space group), and three Bragg peaks with relative positions in a ratio of $\sqrt{2}:\sqrt{4}:\sqrt{6}$, which we indexed as the (1 1 0), (2 0 0), and (2 1 1) reflections of a primitive inverse bicontinuous cubic phase ($Im3\,m$ crystallographic space group) [34]. Structural parameters from SAXS measurements, such as the lattice parameter (a) and the water channel radius (r_W), are reported in Table 1.

DLS results reported in Table 1 showed that the average hydrodynamic diameters of the nanoparticles are in good agreement with that estimated from cryo-TEM images, and the size polydispersity (*i.e.*, the PDIs) and the ζ-potential do not significantly diverge from those reported for similar formulations [20,21].

Formulations here investigated display a negative charge although they are constituted by nonionic molecules. This fact deserves some comments. To exclude the possibility that the negative charge might be ascribed to the presence of MO impurities, a cubosome formulation was prepared using pure (>99%) MO from Sigma Aldrich. This formulation was characterized by an average diameter of the nanoparticles of 133 ± 1 nm and a negative zeta-potential of −16 ± 1 mV. Moreover, also cubosomes formulations

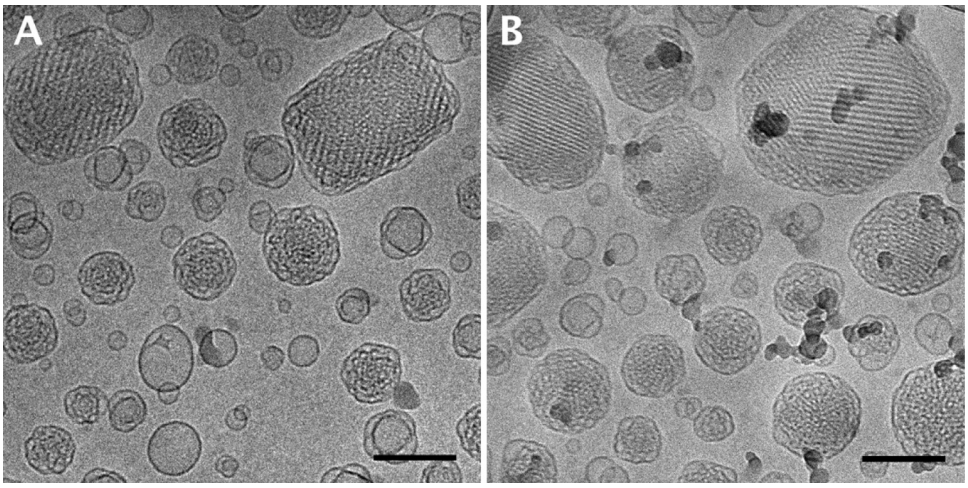

Fig. 1. Cryo-TEM image of monoolein-based cubosome nanoparticles empty (A) or containing the anticancer drug quercetin (B) and prepared using a mixture of PF108 and PF108-D in the ratio 65/35. Small dark globules in B are frost particles. Bars correspond to 100 nm.

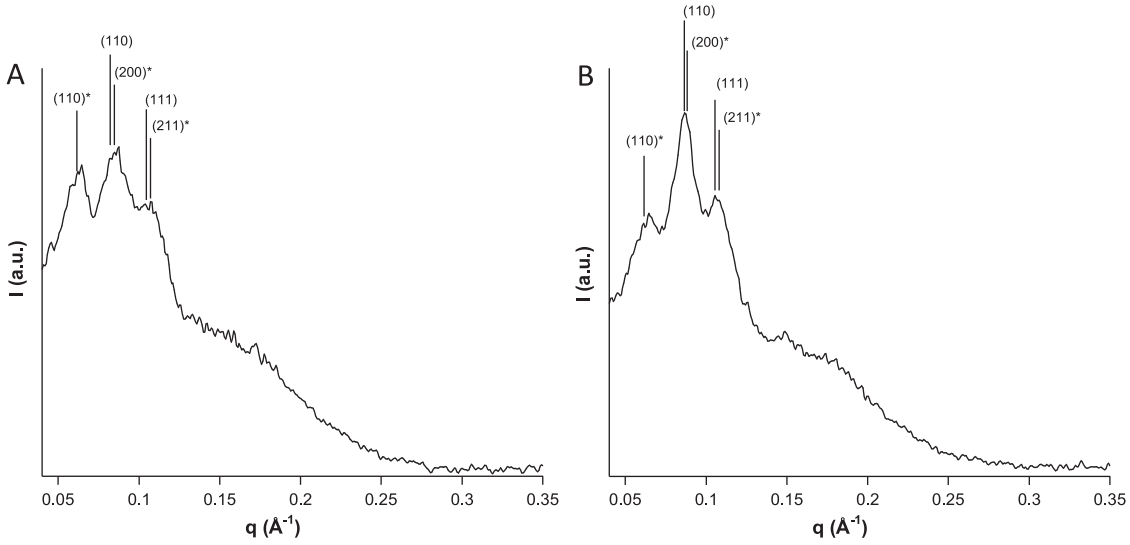

Fig. 2. SAXS diffractograms of monoolein-based cubosome nanoparticles either empty (A) or loaded with quercetin (B) and prepared using a mixture of PF108 and PF108-D in the ratio 65/35. Experiments were performed on samples formulated with 7.2 wt% of the dispersed phase (see also the text).

prepared using phytantriol (3,7,11,15-tetramethylhexadecane-1,2,3-triol) show a negative zeta-potential (about −9 mV) [35]. It should be noticed that, differently from monoolein, this polar lipid does not contain ester bonds that can be hydrolyzed to form a carboxylic acid. Consequently, also the presence of small amounts of acids due to monoolein hydrolysis products (though possible) cannot fully justify the measured zeta-potentials in all these different systems. On the other hand, hydroxide ions adsorption (a phenomenon often observed at the oil/water interface), originating a polarized water layer surrounding the outer surface of the nanoparticles, could explain the observed negative charge [36,37].

As expected, cryo-TEM, SAXS, and DLS analysis confirmed that the presence of the fluorophore molecules in the external polyethylene oxide corona of the cubosomes did not modify the supramolecular morphological features of the colloidal dispersion. Furthermore, after encapsulation of quercetin within the lipid bilayer, the inner nanostructure of the cubosomes was preserved.

3.2. PF108-D, PF108 and fluorescent cubosomes. Physicochemical and photophysical characterization

Before analyzing the UV–visible light emission/absorption characteristics of the new cubosome formulation, the physicochemical and photophysical properties of the pure block copolymers (PF108 and PF108-D) in water were investigated. When dispersed in aqueous solution the PEO–PPO–PEO block copolymers essentially

Table 1
Space groups (in parenthesis), lattice parameters (a), and water channel radii (r_W) obtained from SAXS experiments, mean hydrodynamic diameters (d_H), polydispersity indexes from cumulant analysis (PDI), and ζ-potentials obtained from DLS experiments on the cubosome formulations prepared with a mixture of F108 and F108-D in the 65/35 ratio (wt%). An estimation of the sample stability is also reported. DLS and SAXS experiments were respectively performed on samples formulated with 3.6 and 7.2 wt% of the dispersed phase (see also the text). Errors are reported as ± estimated standard deviation (SD).

Formulation	a (Å)	r_W (Å)	d_H (nm)	PDI	ζ-Potential (mV)	Stability (weeks)
Cubosomes-D	104 ± 1 (Pn3 m)146 ± 1 (Im3 m)	24 ± 128 ± 1	168 ± 1	0.15	−21 ± 1	>24
Cubosomes-D + QUE	102 ± 1 (Pn3 m)143 ± 1 (Im3 m)	23 ± 127 ± 1	171 ± 1	0.14	−23 ± 1	>24

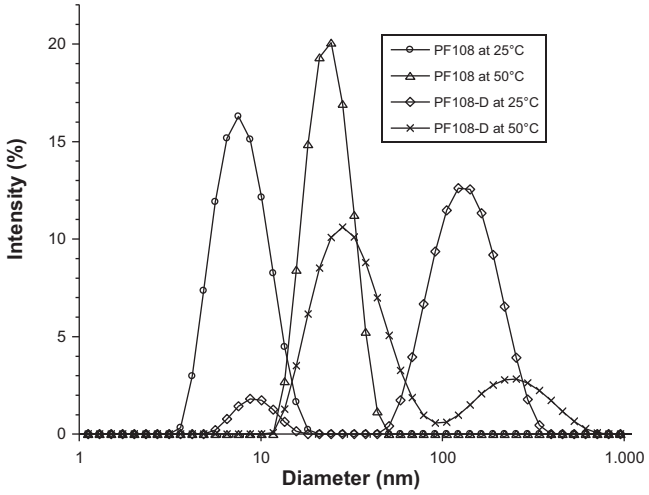

Fig. 3. Intensity-weighted size distributions (expressed in terms of apparent hydrodynamic diameter) obtained from DLS measurements on PF108 and PF108-D solutions with the concentrations of 3.8×10^{-4} and 2.9×10^{-4} M respectively at 25 and 50 °C.

behave like classical surfactants containing PEO. Therefore, above the critical micelle concentration (CMC), these block copolymers self-assemble forming variously shaped (spherical or rod-like depending on the PPO and PEO block length) micelles [38]. These copolymers also present a critical micelle temperature (CMT) due the fact that PPO becomes hydrophobic at higher temperatures. The CMT can be determined using differential scanning calorimetry (DSC) as the DSC signal is related to the change in the hydration of PPO, a process with an endothermic transition enthalpy, which occurs when the micelles are formed [39]. Furthermore, in the same study, it was found that the CMT increases with a decreasing copolymer concentration. However, the description of spherical micelles with a core of dehydrated PPO blocks surrounded by hydrated PEO blocks constituting an outer corona, although useful for explaining most of the experimental data, is quite far from representing the real micellar organization, since water can penetrate the micellar core to some extent, and miscibility of the PEO and PPO blocks is also allowed [40].

Water solutions of PF108 and PF108-D with the concentrations of 3.8×10^{-4} M, and 2.9×10^{-4} M, respectively, were studied at 25 and 50 °C using dynamic light scattering. The intensity-weighted hydrodynamic diameter distributions obtained from the data analysis described above are reported in Fig. 3. The absence of micelles in both solutions at 25 °C was expected because of the low concentrations used, which were well below the CMC at this temperature [41]. In our measurements, the PF108 solution at 25 °C presents a monomodal size distribution with a mean hydrodynamic diameter of 8.1 nm, which can be attributed to the copolymer monomers. When the temperature is raised to 50 °C (above the critical micelle temperature for a PF108 concentration of 3.8×10^{-4} M), the monomodal size distribution shifts to a larger mean diameter of 24.3 nm. This mode can be assigned to micelles of PF108 and the size is in accordance with literature [41], differently from the unmodified copolymer solution, at 25 °C, the PF108-D solution shows a bimodal size distribution characterized by two peaks centered at 8.7 and 137.3 nm, respectively (Fig. 3). Bimodal size distributions are often found in DLS measurements on PEO–PPO–PEO block copolymer solutions with concentrations below CMC or at temperatures below CMT. The two modes are typically related to the simultaneous presence of unimers and clusters. The latter is an effect of the presence of low molecular weight (and more hydrophobic) copolymer fragments, the amount of which can differ between different commercial batches [42,43]. These contaminants become incorporated into the micelles once they are formed, except the most hydrophilic components, that stay in solution [44,45]. Here, this scenario can be ruled out because of the absence of clusters in the PF108 solution (both block copolymers belong from the same batch). It is rather the hydrophobic interactions between the dansyl moieties that may play an important role in the formation of aggregates of PF108-D. This can justify the existence of a second slow mode in the distribution. The DLS results for the PF108-D solution at 50 °C also reveal two modes, one corresponding to a hydrodynamic mean diameter of 26.2 nm and one to 150.5 nm. The fast mode is attributed to PF108-D micelles, whereas the slower one could possibly be related to aggregates of some sort (however, not to unimer clusters as discussed above). It is worth noticing that they are very few in numbers, but could well be the effect of an ill-set base line in the calculations. Indeed, this peak was found strongly affected by a base line contribution (several measurements were performed). An evidence of their low number is given in Fig. S1 (Supplementary data), where the same size distribution presented in Fig. 3 is reported as number-averaged instead of intensity-averaged.

As a concluding remark, DLS results evidenced that conjugation of the dansyl moiety to the end of the PF108 arms significantly alter the self-assembling properties of this block copolymer.

Dansyl is a hydrophobic naphthalene derivative showing a fluorescence emission that shifts bathocromically as the polarity of the surrounding medium increases. Therefore, fluorescence spectroscopy studies can give important information about the environment experienced by this molecule. The absorption spectrum of PF108-D showed an absorption band at 247 nm ($\varepsilon = 30{,}168\ M^{-1}cm^{-1}$) and a less intense band at 344 nm ($\varepsilon = 7980\ M^{-1}cm^{-1}$) as shown in Fig. 4A. Upon excitation at 344 nm, an emission band centered at 532 nm ($\Phi = 4.25 \times 10^{-3}$) was observed, as shown in Fig. 4B. Previous studies on the dansyl molecule reported a fluorescence emission maximum, which shifts from 494 nm when dispersed in a 10% Pluronic L62 ($EO_6PO_{36}EO_6$) water solution (where the dye preferentially resides in the micelle hydrophobic core) to about 529 nm when the dispersion medium was a tetraethylene glycol/water mixture (used to mimic the micellar PEO corona) [46]. Moreover, Bright and co-workers [47], showed that in a dendrimeric family functionalized with a dansyl moiety increase in dendrimers generation (from the first to the third) caused a hypsochromic shift in the fluorophore emission (547 nm, 542 nm, and 535 nm, for the first, second, and third generation, respectively) as a result of a less polar microenvironment surrounding the dansyl group. These results are also in accordance with those reported in the literature for a dansyl group attached to dendrimers [47,48], silica nanoparticles [49], or cyclodextrines [50]. Consequently, the emission observed in the aqueous solution of the PF108-D can be considered a robust evidence that, rather than completely exposed to the water molecules, the fluorogenic fragments experience a less polar environment mainly constituted by the EO groups.

The absorption spectrum of the cubosomes formulation prepared using the mixture of PF108 and PF108-D as a stabilizer could not be recorded due to the intense scattering of the sample. However, when excited at 344 nm, an emission band at 531 nm was found. The similarity of this emission band with that observed in the PF108-D aqueous solution strongly suggests that the fluorogenic fragments are at least partially buried within the PEO corona.

3.3. *Fluorescent cubosome internalization and cytotoxic features against HeLa cells*

The fluorescent cubosome formulation was then investigated *in vitro* to test cellular internalization and cytotoxicity features in HeLa cell culture. Fig. 5A shows the optical images which highlight

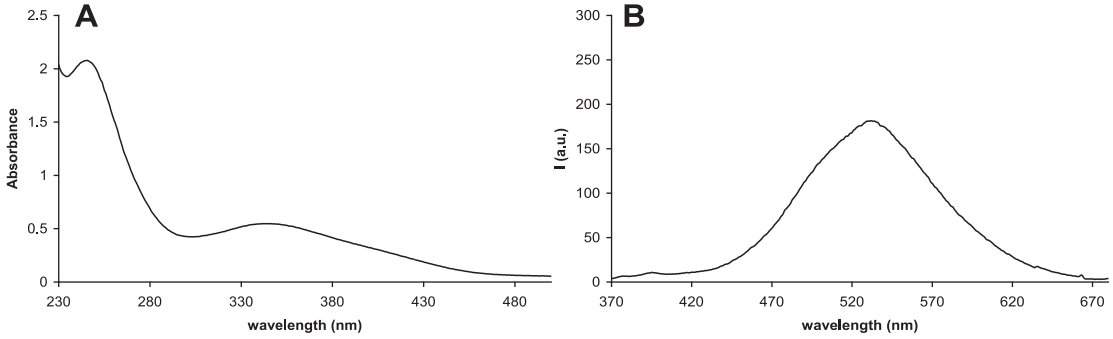

Fig. 4. Absorption (A) and emission (B) spectra (λ_{exc} = 344 nm, λ_{em} = 532 nm) of a 6.9×10^{-5} M water solution of PF108-D.

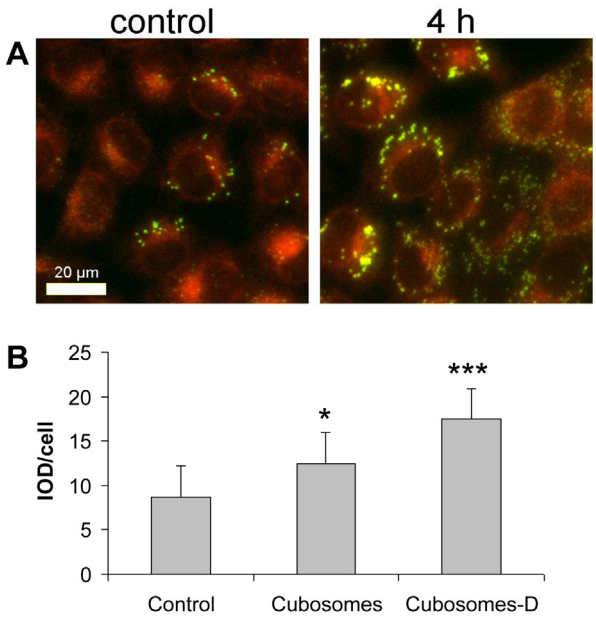

Fig. 5. Lipid droplet accumulations induced in HeLa cells by cubosome treatment. (A) Representative composite color images of HeLa cells exposed to monoolein-based cubosomes (without quercetin loading) at 4 h incubation. Membranes (red) and lipid droplets (green) were stained with Nile Red. (B) IOD (integrated optical density) per cell related to lipid droplet accumulation in HeLa cells exposed to lipid-based cubosomes. Data are expressed as mean ± SD from at least two independent experiments. Lipid droplet quantification was performed with Image Pro Plus. * and *** represent $p < 0.05$ and $p < 0.001$ *versus* control, respectively.

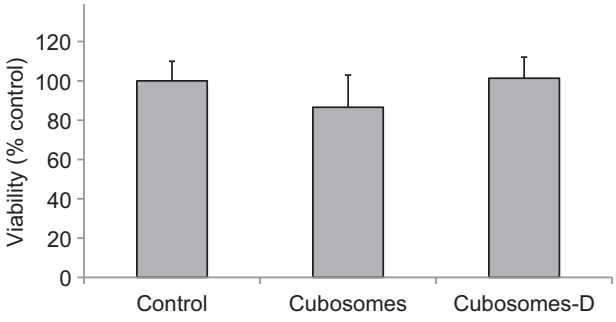

Fig. 6. Viability, expressed as % of the control, induced by incubation for 4 h with lipid-based cubosomes (1:500, 2 μl/ml) in HeLa cells culture. Three independent experiments were performed and data are presented as mean ± SD (n = 12).

the lipid droplet accumulation in HeLa cells as a result of cubosome treatment.

The lipid droplets (LDs), cytoplasmic organelles involved in the controlled synthesis and mobilization of fat stores, consist of a phospholipid monolayer surrounding a hydrophobic core of neutral lipids [51]. Although marked differences in terms of size, number, and lipid content, are observed from one cell type to another [52], their increase basically occurs because of exogenous lipids uptake. Indeed, cell internalization exposes cubosomes to endosomal/lysosomal degradation into the single components (MO and the block copolymer), with a consequent redistribution of the lipids between the cytoplasmic membranes and the lipid droplets. Therefore, the amount of LDs straightforwardly reflect the internalization of the cubosomes *via* endocytosis pathway, and LDs accumulation can be used, at least in principle, to validate the cellular uptake of all kinds of lipid-based nanoparticles. Accordingly, LDs accumulation following monoolein-based nanoparticles (vesicles or cubosomes) administration was previously reported [20,53]. Here, the lipid droplet growth caused by the internalization of two cubosome formulations (not carrying the quercetin) prepared with PF108 or with the PF108/PF108-D mixture was confirmed and quantified *via* estimation of the IOD (integrated optical density) per cell. An increased production of lipid droplets was observed for both nanoparticles at 4 h of incubation time in comparison with untreated-control cells, as shown in Figs 5A and B. Results evidenced a statistically different IOD/cell between nanoparticle formulations, very likely caused by the dansyl moieties exposed on the surface of the cubosomes. Indeed, dansyl may to some extent, alter the molecular recognition characteristics of the cubosomes' surface, changing their interactions with the cells.

The two aforementioned nanoparticle formulations were also tested for cytotoxicity (MTT assay) in HeLa cells. Fig. 6 shows the viability, expressed as % of the control, induced in HeLa cells after 4 h incubation, and evidences that treatments with both nanoparticle formulations did not induce a relevant reduction in cell viability in comparison with control cells.

4. Conclusions

When dealing with soft matter based nanoparticles (such as cubosomes or hexosomes), one of the issues researchers working in the field of nanomedicine have to face is the preservation of their morphology and internal structure after cargos loading. To overcome this problem, we proposed here a strategy that considers the conjugation of a fluorescence probe, namely dansyl, to the end of the hydrophilic arms of the PEO–PPO–PEO block copolymer PF108, which is used to stabilize an aqueous dispersion of monoolein-based cubosomes. In this way, both the morphology and topology were not significantly altered by the presence of the fluorescent molecules.

The physicochemical investigation presented here demonstrate that a mixture of this new fluorescently labeled block copolymer PF108-D and the original PF108 copolymer is effective in stabilizing in water the cubosome formulation also encapsulating the anticancer drug quercetin. The performed steady-state fluorescence

and UV–vis experiments evidenced good photophysical properties of such a formulation, while the microscopic observations on HeLa cell cultures proved their effective internalization and high biocompatibility (when not carrying the drug), when used at the same concentration suitable for imaging purposes.

Taken on the whole, the results presented in our study validate the potential use of this new cubosome formulation in theranostic nanomedicine.

Acknowledgements

Financial support by MIUR (Project PRIN 2010BJ23MN_002) and Regione Autonoma della Sardegna (CRP-59699) is gratefully acknowledged. Sardegna Ricerche Scientific Park (Pula, CA, Italy) is acknowledged for free access to facilities of the Nanobiotechnology Laboratory. The cryo-TEM work was performed at the Technion Laboratory for Electron Microscopy of Soft matter, supported by the Technion Russell Berrie Nanotechnology Institute (RBNI). K. Schillén acknowledges the Swedish Research Council (VR) for financial support.

Appendix A. Supplementary data

Supplementary data associated with this article can be found, in the online version, at http://dx.doi.org/10.1016/j.colsurfb.2015.03.025.

References

[1] K.Y. Choi, G. Liu, S. Lee, X. Chen, Nanoscale 4 (2012) 330–342.
[2] S.M. Janib, A.S. Moses, J.A. MacKay, Adv. Drug. Deliv. Rev. 62 (2010) 1052.
[3] T. Lammers, S. Aime, W.E. Hennink, G. Storm, F. Kiessling, Acc. Chem. Res. 44 (2011) 1029.
[4] S. Svenson, Mol. Pharm. 10 (2013) 848–856.
[5] S.S. Kelkar, T.M. Reineke, Bioconjug. Chem. 22 (2011) 1879.
[6] H. Wang, Y. Wu, R. Zhao, G. Nie, Adv. Mater. 25 (2013) 1616–1622.
[7] S.T. Hyde, J. Phys. Chem. 93 (1989) 1458–1464.
[8] K. Larsson, Nature 304 (1983) 664.
[9] K. Larsson, J. Phys. Chem. 93 (1989) 7304–7314.
[10] S. Hyde, S. Andersson, K. Larsson, Z. Blum, T. Landh, S. Lidin, B.W. Ninham, The Language of Shape, Elsevier, Amsterdam, 1997.
[11] Z.A. Almsherqi, S.D. Kohlwein, Y. Deng, J. Cell Biol. 173 (2006) 839–844.
[12] Z.A. Almsherqi, T. Landh, S.D. Kohlwein, Y. Deng, Int. Rev. Cell Mol. Biol. 274 (2009) 275–342.
[13] S. Murgia, S. Lampis, P. Zucca, E. Sanjust, M. Monduzzi, J. Am. Chem. Soc. 132 (2010) 16176–16184.
[14] T. Landh, J. Phys. Chem. 98 (1994) 8453–8467.
[15] X. Mulet, B.J. Boyd, C.J. Drummond, J. Colloid Interface Sci. 393 (2013) 1–20.
[16] J. Barauskas, M. Johnsson, F. Tiberg, Nano Lett. 5 (2005) 1615–1619.
[17] D.P. Chang, M. Jankunec, J. Barauskas, F. Tiberg, T. Nylander, Langmuir 28 (2012) 10688–10696.
[18] B.W. Muir, D.P. Acharya, D.F. Kennedy, X. Mulet, R.A. Evans, S.M. Pereira, L.K. Wark, B.J. Boyd, T.-H. Nguyen, T.M. Hinton, J.L. Waddington, N. Kirby, D.K. Wright, H.X. Wang, F.G. Egan, B.A. Moffat, Biomaterials 33 (2012) 2723.
[19] C. Nilsson, B. Barrios-Lopez, A. Kallinen, P. Laurinmäki, S.J. Butcher, M. Raki, J. Weisell, K. Bergström, S.W. Larsen, J. Østergaard, C. Larsen, A. Urtti, A.J. Airaksinen, A. Yaghmur, Biomaterials 34 (2013) 8491–8503.
[20] C. Caltagirone, A.M. Falchi, S. Lampis, V. Lippolis, V. Meli, M. Monduzzi, L. Prodi, J. Schmidt, M. Sgarzi, Y. Talmon, R. Bizzarri, S. Murgia, Langmuir 30 (2014) 6228–6236.
[21] S. Murgia, S. Bonacchi, A.M. Falchi, S. Lampis, V. Lippolis, V. Meli, M. Monduzzi, L. Prodi, J. Schmidt, Y. Talmon, C. Caltagirone, Langmuir 29 (2013) 6673–6679.
[22] K. Larsson, J. Disp. Sci. Technol. 20 (1999) 27–34.
[23] http://www.fda.gov/Food/IngredientsPackagingLabeling/GRAS/SCOGS/ucm260418.htm
[24] J.A. Barreto, W. O'Malley, M. Kubeil, B. Graham, H. Stephan, L. Spiccia, Adv. Mater. 23 (2011) H18.
[25] J.C. Bodea, J. Kuntscheb, S.S. Funaric, H. Bunjes, Int. J. Pharm. 448 (2013) 87–95.
[26] W. Leesajakul, M. Nakano, A. Taniguchi, T. Handa, Colloids Surf. B 34 (2004) 253–258.
[27] R. Angius, S. Murgia, D. Berti, P. Baglioni, M. Monduzzi, J. Phys. Condens. Matter 18 (2006) S2203.
[28] Y. Talmon, Ber. Bunsenges. Phys. Chem. 100 (1996) 362–372.
[29] J. Janiak, S. Bayati, L. Galantini, N.V. Pavel, K. Schillén, Langmuir 28 (2012) 16536–16546.
[30] J.F. Miller, K. Schätzel, B. Vincent, J. Colloid Interface Sci. 143 (1991) 532–554.
[31] B.J. Frisken, Appl. Opt. 40 (1991) 4087–4090.
[32] Y. Long, J.Y.N. Philip, K. Schillén, F. Liu, L. Ye, J. Mol. Recognition 24 (2011) 619–630.
[33] J. Briggs, H. Chung, M. Caffrey, J. Phys. II France 6 (1996) 723–751.
[34] S. Murgia, A.M. Falchi, M. Mano, S. Lampis, R. Angius, A.M. Carnerup, J. Schmidt, G. Diaz, M. Giacca, Y. Talmon, M. Monduzzi, J. Phys. Chem. B 114 (2010) 3518–3525.
[35] Q. Liu, Y.-D. Dong, T.L. Hanley, B.J. Boyd, Langmuir 29 (2013) 14265–14273.
[36] J.K. Beattie, A.M. Djerdjev, Angew. Chem. Int. Ed. (2004) 43.
[37] C.D. Driever, X. Mulet, L.J. Waddington, A. Postma, H. Thissen, F. Caruso, C.J. Drummond, Langmuir 29 (2013) 12891–12900.
[38] K. Mortensen, J. Phys. Condens. Matter 8 (1996) A103–A124.
[39] R.C. da Silva, G. Olofsson, K. Schillén, W. Loh, J. Phys. Chem. B 106 (2002) 1239–1246.
[40] P. Linse, M. Malmsten, Macromolecules 25 (1992) 5434–5439.
[41] P. Alexandridis, T. Nivaggioli, T.A. Hatton, Langmuir 11 (1995) 1468–1476.
[42] W. Brown, K. Schillén, S. Hvidt, J. Phys. Chem. 96 (1992) 6038–6044.
[43] J. Jansson, K. Schillén, G. Olofsson, R. Cardoso da Silva, W. Loh, J. Phys. Chem. B 108 (2004) 82–92.
[44] W. Batsberg, S. Ndoni, C. Trandum, S. Hvidt, Macromolecules 37 (2004) 2965–2971.
[45] S. Hvidt, W. Batsberg, Int. J. Polym. Anal. Charact. 12 (2007) 13–22.
[46] M. Vasilescu, R. Bandula, H. Lemmetyinen, Colloid Polym. Sci. 288 (2010) 1173–1184.
[47] C.M. Cardona, J. Alvarez, A.E. Kaifer, T. Donovan Mc Carley, S. Pandey, G.A. Baker, N.J. Bonzagni, F.V. Bright, J. Am. Chem. Soc. 122 (2000) 6139–6144.
[48] F. Vögtle, S. Gestermann, C. Kauffmann, P. Ceroni, V. Vicinelli, L. De Cola, V. Balzani, J. Am. Chem. Soc. 121 (1999) 12161–12166.
[49] J. Isaad, A. El Achari, Tetrahedron 69 (2013) 4866–4874.
[50] H.F.M. Nelissen, F. Venema, R.M. Uittenbogaard, M.C. Feiters, R.J.M. Nolte, J. Chem. Soc. Perkin Trans. 2 (1997) 2045–2053.
[51] S. Martin, R.G. Parton, Nat. Rev. Mol. Cell Biol. 7 (2006) 373–378.
[52] M. Digel, R. Ehehalt, J. Fullekrug, FEBS Lett. 584 (2010) 2168–2175.
[53] M. Carboni, A.M. Falchi, S. Lampis, C. Sinico, M.L. Manca, J. Schmidt, Y. Talmon, S. Murgia, M. Monduzzi, Adv. Healthcare Mater. 2 (2013) 692–701.